Radiation Physics and Chemistry 166 (2020) 108427

Contents lists available at ScienceDirect

Radiation Physics and Chemistry

journal homepage: www.elsevier.com/locate/radphyschem

# Calculation of S-values for head and brain structures from a constructed voxelized phantom for positron-emitting radionuclides

C.A. Reynoso-Mejía[a,b,*], N. Kerik-Rotenberg[b], M. Moranchel[a]

[a] Escuela Superior de Física y Matemáticas, Av. Instituto Politécnico Nacional s/n San Pedro Zacatenco, Mexico City, C.P. 07738, Mexico
[b] Instituto Nacional de Neurología y Neurocirugía Manuel Velasco Suárez, Av. Insurgentes Sur No. 3877, La Fama, Mexico City, C.P. 14269, Mexico

ARTICLE INFO

*Keywords:*
Computational phantoms
Positron emission tomography
Monte Carlo simulation
S-values

ABSTRACT

Stylized and voxelized phantoms have been used to estimate S-values for positron-emitting radionuclides. However, there is a lack of computational phantoms that include head and brain structures of importance for neuroimaging studies, such as brain PET-CT. The aim of this work was to construct a multi-resolution whole-body phantom for Monte Carlo simulations in MCNP code that includes a complete set of head and brain structures. The International Commission on Radiological Protection (ICRP-110) male reference phantom and the Zubal head phantom were used to construct the ICRP-HEAD phantom. This multi-resolution phantom was used to calculate self-absorbed fractions (SAFs) and S-values for seven positron-emitting radionuclides used in PET neuroimaging (C-11, O-15, F-18, Cu-64, I-124, Ga-68, and Y-86). S-values calculated in this work were compared with two head/brain phantoms previously published: the stylized MIRD-15 phantom and the tomographic VIP-Man phantom. The voxel resolution of the phantom resulted well suited for Monte Carlo simulations in MCNP6.2 code. For the same target and source structure, the highest auto absorbed S-values were produced by O-15 and Ga-68, while for different target and source structures, Y-86 produced the highest S-values. The lowest S-values were produced by Cu-64. Comparison of S-values with those calculated from the MIRD-15 phantom showed significant differences, while a better agreement was found with those calculated from the VIP-Man phantom. The S-values obtained in this work could help to improve the accuracy of absorbed dose in brain and head structures for positron-emitting radionuclides used in PET neuroimaging.

## 1. Introduction

Neuroimaging studies such as brain positron emission tomography (PET) combined with computed tomography (CT) allow to visualize the brain anatomy and to quantify several biochemical and metabolic processes. Brain PET-CT is used to detect diseases such as Alzheimer, dementias, movement disorders, Parkinson, stroke, epilepsy, and brain tumors (Tai, 2004). In addition to its clinical applications, PET is increasingly used for clinical research and drug discovery and development. Due to this, and considering that some head and brain structures are highly radiosensitive (Emami et al., 1991), to estimate the absorbed dose in brain structures could help to assess the associated risk as well as to the optimization of neuroimaging PET-CT studies.

The estimation of absorbed dose due to use of radiopharmaceuticals depends on the calculation of S-values which are derived from Monte Carlo simulations of radiation transport on computational phantoms, according to the Committee on Medical Internal Radiation Dose (MIRD) (Loevinger et al., 1991). Computational phantoms are representations of the organs or structures of the human body with defined shape, volume, composition, and density (Xu and Eckerman, 2009); they can be categorized in stylized, tomographic, and deformable phantoms. Stylized phantoms are created with a combination of geometrical shapes from simple equations. Voxelized phantoms are obtained from medical images, such as CT or magnetic resonance (MR). Deformable phantoms are based on a polygon mesh surfaces or non-Uniform Rational B-Splines (NURBS) surfaces and they can be deformed to change their shape and size.

A few studies have calculated S-values for head and brain structures for positron-emitting radionuclides with realistic anthropomorphic phantoms. The OLINDA/EXM Version 1.0 software is based on the stylized MIRD-15 head phantom that includes 14 brain structures and it was used to calculate S-values for 24 radionuclides (Bouchet et al., 1999). Although the MIRD-15 head phantom is not completely realistic since the brain anatomy is difficult to reproduce with simple geometric

* Corresponding author. Escuela Superior de Física y Matemáticas, Av. Instituto Politécnico Nacional s/n San Pedro Zacatenco, Mexico City, C.P. 07738, Mexico.
*E-mail addresses:* betoven@ciencias.unam.mx, creynosom1401@alumno.ipn.mx (C.A. Reynoso-Mejía), nora.kerik@hotmail.com (N. Kerik-Rotenberg), mmoranchel1508@gmail.com (M. Moranchel).

https://doi.org/10.1016/j.radphyschem.2019.108427
Received 26 February 2019; Received in revised form 17 July 2019; Accepted 20 July 2019
Available online 22 July 2019
0969-806X/ 

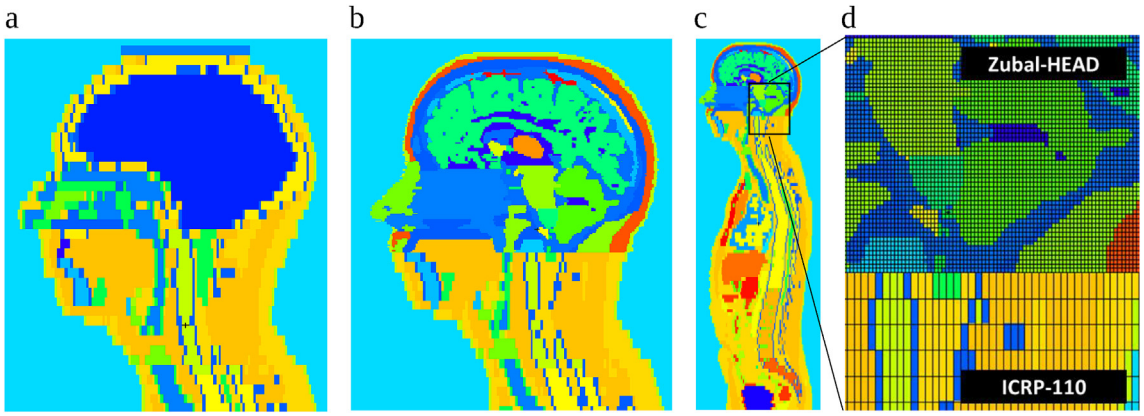


**Fig. 1.** (a) The original ICRP-110 adult male reference phantom, (b) the constructed ICRP-HEAD phantom that includes the head and brain structures, (c) the ICRP-HEAD phantom with head/brain and body, and (d) the region in the black rectangle shown in (c), indicating the interface region between the computational phantoms used to construct the ICRP-HEAD phantom and showing the differences in resolution.

structures, it has been the standard phantom used to estimate absorbed dose. The voxelized Visible Photographic Man (VIP-Man) phantom has been used to calculate S-values for 15 head and brain structures for 5 radionuclides with EGS4 Monte Carlo code (Chao and Xu, 2004); however, this phantom does not correspond to a reference adult male phantom as defined in the International Commission on Radiological Protection (ICRP) publication 89 (Valentin, 2002). The OLINDA/EXM Version 2.0 software includes S-values calculated from an adult male phantom with organ and tissue masses according to the ICRP-89 created from NURBS surfaces (XCAT phantom) (Segars et al., 2010); however, only few head and brain structures were considered in this software (brain, eyes, and salivary glands), which reduces its use to estimate absorbed dose in neuroimaging studies (Stabin and Siegel, 2018). Furthermore, the ICRP-110 reference phantoms, based on ICRP-89 reference tissues, only include the brain, eyes, pituitary gland, and salivary glands organs (Menzel et al., 2009).

Although deformable phantoms are more realistic than stylized phantoms, they must be converted into voxel-based phantoms in order to perform Monte Carlo simulations of radiation transport. The resolution of a phantom is limited by the maximum number of voxels which a Monte Carlo code can work with, and it depends on the computational memory. Thus, the typical resolution of a phantom is a few millimeters (Caracappa et al., 2014). For this reason, the voxel-based phantoms have limitations in representing small structures as those of head and brain. The Zubal head phantom is a computationally efficient model for Monte Carlo N-Particles (MCNP) code due to its resolution; it represents the head and brain of a standard adult male and it contains 64 brain structures (Zubal et al., 1994). The Zubal head phantom has been widely used in medical physics research, but it has not been used to estimate S-values (Evans et al., 2001)(My et al., 2010)(Jia et al., 2012).

The aim of this work was to construct a multi-resolution whole-body phantom for Monte Carlo simulations in MCNP6.2 that includes a complete set of head and brain structures. This phantom, called ICRP-HEAD phantom, was based on the ICRP-110 adult male reference phantom and on the Zubal head phantom, and it was used to calculate self-absorbed fractions (SAFs) and S-values for 7 positron-emitting radionuclides relevant in PET neuroimaging (C-11, O-15, F-18, Cu-64, I-124, Ga-68, and Y-86). S-values for 16 source structures and 20 target structures were calculated, including structures such as brainstem, putamen, lentiform nucleus, complete spinal cord, lenses, thyroid, pharynx, parotid glands, pituitary gland, and lacrimal glands. S-values calculated with the ICRP-HEAD phantom were compared with those obtained from the VIP-Man phantom and the stylized MIRD-15 head phantom. The constructed phantom is freely available to other investigators upon request.

## 2. Materials and method

### 2.1. Computational phantom

In order to create a phantom with low computational cost for Monte Carlo simulations in MCNP code with the main structures of the head and brain, a multi-resolution voxel phantom was created based on the Zubal head phantom and on the ICRP-110 adult male reference phantom. The Zubal head phantom was modified and inserted in the head part of the ICRP-110 reference phantom. The phantom with two different resolutions was constructed by incorporating repeated structures based on rectangular lattices and designating universes for each structure. Two lattices of different scales were used to construct the body and head of the phantom. The constructed phantom contains 62 structures in the head/brain region with a voxel resolution of $1.1 \times 1.1 \times 1.4\,\mathrm{mm}^3$ while the body part consists of 140 segmented organs with a resolution of $2.137 \times 2.137 \times 8\,\mathrm{mm}^3$. The material composition and densities of the body and brain structures were obtained from ICRP-89 (Valentin, 2002), ICRU-46 (White et al., 1992) and Evans et al. (2001). Fig. 1 shows a comparison between the original ICRP-110 adult male reference phantom and the constructed ICRP-HEAD phantom.

### 2.2. Absorbed dose calculation

According to MIRD pamphlet 21 (Bolch et al., 2009) the mean absorbed dose $D(r_T, T_D)$ to the target-tissue $r_T$ from source-tissue $r_S$ over a dose-integration period $T_D$ after administration of the radiopharmaceutical is given as:

$$D(r_T, T_D) = \sum_{r_S} \int_0^{T_D} A(r_S, t) S(r_T \leftarrow r_S, t) dt, \tag{1}$$

$A(r_S, t)$ is the cumulated activity of the radiopharmaceutical, which is obtained by longitudinal PET or SPECT images, the S-values $S(r_T \leftarrow r_S, t)$ are obtained from Monte Carlo simulations and represent the mean absorbed dose rate to target-tissue from the source-tissue per unit activity. S-values are defined by:

$$S(r_T \ r_S, t) = \frac{1}{M_T} \sum_i E_i Y_i \varphi(r_T r_S, E_i), \tag{2}$$

$E_i$ is the individual energy of the $i$*th* nuclear transition, $Y_i$ is number of $i$*th* nuclear transitions per nuclear transformation, $M_T$ is the mass of the target-tissue, and $\varphi(r_T r_S, E_i)$ is the absorbed fraction (AF). The AF is defined as the proportion of energy deposited in the target-tissue from the source-tissue. When the target-organ and the source-organ are the same, the AF is called self-absorbed fraction (SAF), while when the

**Table 1**
Source and target organs used to calculate S-values.

| Source-organs | Target-organs |
|---|---|
| Caudate nucleus | Caudate nucleus |
| Cerebellum | Cerebellum |
| Cerebral cortex | Cerebral cortex |
| Corpus callosum | Corpus callosum |
| Pons and midbrain | Medulla oblongata |
| Brainstem | Pons and midbrain |
| Putamen | Brainstem |
| Thalamus | Optic nerve |
| Cerebral white matter | Putamen |
| Lacrimal gland | Spinal cord |
| Parotid gland | Thalamus |
| Pituitary gland | Cerebral white matter |
| Lentiform nucleus | Eyes |
| Skull | Lenses |
| Lateral ventricles | Lacrimal gland |
| Cerebral fluid | Parotid gland |
| - | Pituitary gland |
| - | Thyroid |
| - | Lentiform nucleus |
| - | Pharynx |

target-organ and the source-organ are different, it is called AF for cross-irradiation.

### 2.3. Monte Carlo simulations

The Monte Carlo N-Particles (MCNP) code version 6.2 was used to simulate radiation transport in the ICRP-HEAD phantom and to calculate SAFs and S-values for head and brain structures. MCNP is a general-purpose Monte Carlo code capable of simulating particle interactions of 36 types of particles and several heavy ions (Werner et al., 2018). Some authors have reported S-values obtained by MCNP simulations for positron-emitting radionuclides for different computational phantoms (adults body phantoms, pediatric phantoms, pregnant/fetus female models, and small animals) (Belinato et al., 2017)(Xie and Zaidi, 2016) (Kinase and Saito, 2007).

In this work, positrons, electrons, and photons were simulated to be uniformly distributed within the source-structure and emitted isotropically. Table 1 shows the list of the head and brain structures considered as source-structures and target-structures. The energy spectra of radionuclides were chosen according to the decay data from the Brookhaven National Laboratory database available from the RADAR website https://www.doseinfo-radar.com/RADARDecay.html (Stabin and da Luz, 2002). The number of particle stories was $6 \times 10^7$, the simulations were performed in a 16 GB RAM computer. Relative standard deviations less than 1% were obtained in almost all simulations, only for some small structures (such as pituitary gland), relative standard deviations less than 3% were obtained. All physical processes were considered by choosing the photon–electron mode (mode p e) with cut-off energy of 1 keV for electrons and for photons.

SAFs and S-values were calculated by using the *F8 tally which gives the energy deposition in MeV. The SAFs for electrons, photons, and positrons were calculated for discrete values of energy (0.01–4.0 MeV) as $^{*}F8/E_0$, where $E_0$ is the emitted energy from the source-structure in MeV. S-values (mGy/MBq*s) for seven positron-emitting radionuclides (C-11, O-15, F-18, Cu-64, I-124, Ga-68, and Y-86) were calculated using the *F8 tally for each target-structure, which was converted to Joules and divided by the mass of the target-structure. In order to compare S-values calculated in this work with those previously published by MIRD-15 and by Chao and Xu (VIP-Man phantom) (Chao and Xu, 2004), ratios of S-values were obtained for those source/target organs and radionuclides common to the mentioned phantoms.

**Table 2**
Comparison of the mass of structures and organs for MIRD-15, VIP-Man, and ICRP-HEAD phantoms.

| Structure | ICRP-89/ICRP-32 reference values (g) | ICRP-HEAD phantom (g) | MIRD-15 phantom (g) | VIP-Man phantom (g) |
|---|---|---|---|---|
| Brain | 1450.0 | 1412.9 | 1512.9 | – |
| Cerebellum | 150.0 | 153.1 | 144.5 | 122.7 |
| Thyroid | 20.0 | 20.8 | 20.7 | 27.6 |
| Eyes | 15.0 | 16.0 | 14.1 | 14.9 |
| Pituitary gland | 0.6 | 0.6 | – | – |
| Brainstem | 30.0 | 28.3 | – | – |
| Lenses | 0.4 | 0.4 | – | 0.5 |
| Spinal cord | 30.0 | 36.8 | 7.0 | – |
| Parotid | 50.0 | 48.6 | – | – |
| Cranium | 1013.9 | 1007.4 | 700.0 | – |
| Optic nerve | – | 1.4 | – | 1.8 |
| Caudate Nucleus | – | 10.9 | 10.9 | 9.0 |
| Cerebral Cortex | – | 655.9 | 646.7 | 681.4 |
| Thalamus | – | 12.9 | 16.3 | 8.1 |
| Cerebral White Matter | – | 513.0 | 674.3 | 440.5 |
| Lentiform Nucleus | – | 15.0 | 20.2 | 13.4 |
| Pons and middle | – | 23.8 | – | 24.6 |
| Corpus Callosum | – | 11.7 | – | 16.9 |
| Lateral ventricles | – | 9.3 | 20.9 | 7.1 |

## 3. Results

The comparison of the mass of the head and brain structures of the MIRD-15, the VIP-Man, and the ICRP-HEAD phantoms are shown in Table 2. The structures of the ICRP-HEAD phantom have similar masses to those recommended by ICRP-89.

### 3.1. Self-absorbed fraction

Fig. 2 shows the SAFs for electrons, photons, and positrons for five brain structures with different masses (cerebral cortex, cerebellum, caudate nucleus, brainstem, and pituitary gland). The SAFs show a clear dependence with the mass of the structures, namely, SAFs increase for structures with large masses.

An expected behavior was found for electrons at low energies, i.e., SAFs are equal to 1 since all energy emitted from the source-structure is auto absorbed. As the source energy increases (up to 100 keV) some electrons leave the source-structure, mainly in structures with small masses such as the pituitary gland, so SAFs decrease.

SAFs for photons decrease rapidly as photon energy increases since they easily come out of the source-tissue. For photon energies higher than 0.1 MeV, less than 10% of the energy emitted from the source-structures is auto absorbed as shown in Fig. 2b.

On the other hand, SAFs for positrons were higher than 1 for energies below 1 MeV, due to the fact that positrons, as well as some annihilation-gamma photons, are absorbed in the source-structure. For energies above 1 MeV, SAFs decrease below 1 since some positrons come out of the source-structure.

### 3.2. S-values for positron-emitting radionuclides

Tables 1–16 in the supplementary material show the S-values calculated for seven positron-emitting radionuclides (C-11, O-15, F-18, Cu-64, I-124, Ga-68, and Y-86) for the source/target structures. As expected, the highest S-values were found when the source and the target structure were the same (auto absorbed S-values). Fig. 3a and b shows bar-graphs of the auto absorbed S-values, and S-values from cerebral cortex as source-organ, respectively. Similar results were obtained for all organs, however, to allow a better visualization, only seven organs with similar masses are shown.

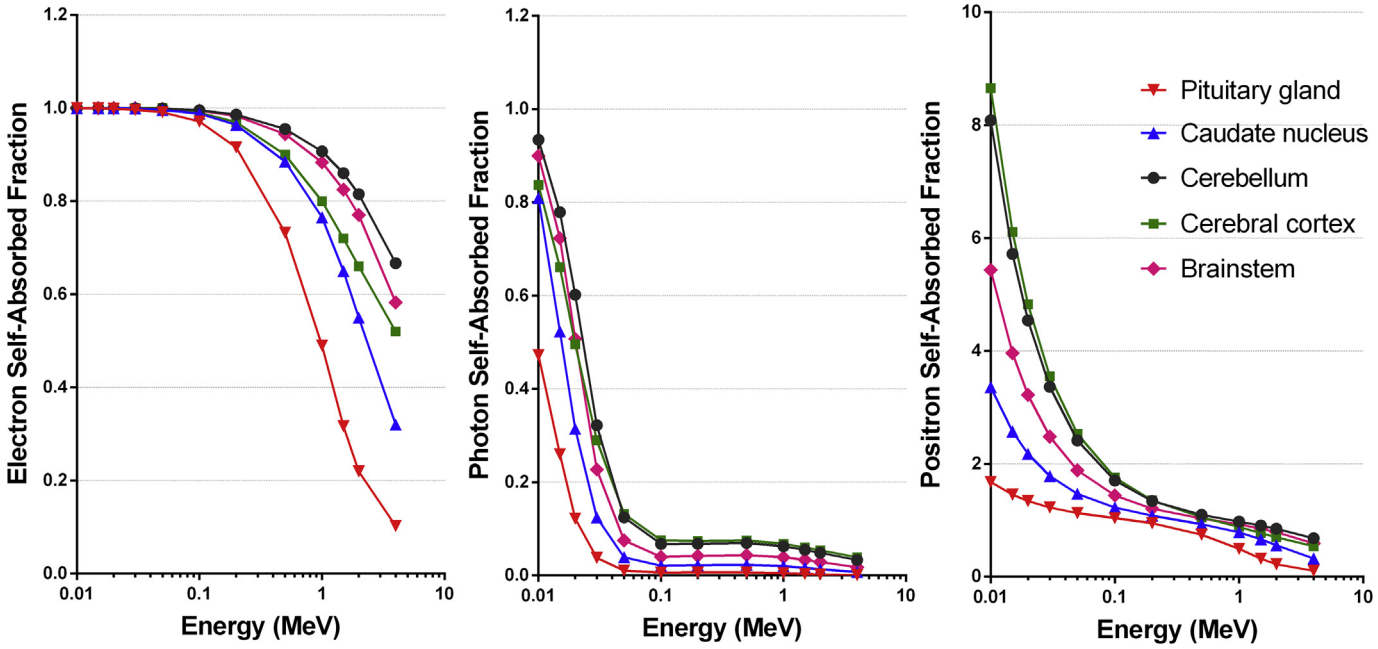


**Fig. 2.** (a) SAFs for electrons, (b) photons, (c) and positrons for five brain structures, cerebral cortex ■, cerebellum ●, caudate nucleus ▲, brainstem ♦, and pituitary gland ▼. Tables 17–19 in the supplementary material show the SAFs data.

For the same target and source organ, the highest auto absorbed S-values were produced by O-15 and Ga-68, while for different target and source organs, Y-86 produced the highest S-values. The lowest S-values were found for Cu-64.

### 3.3. Comparison of S-Values with MIRD-15 and VIP-Man phantoms

Fig. 4 shows the ratios of S-values of the ICRP-HEAD phantom to the stylized MIRD-15 and to the voxelized VIP-Man phantom. The ratios were obtained for eight target-structures (caudate nucleus, cerebellum, cerebral cortex, eyes, lentiform nucleus, thalamus, thyroid, and cerebral white matter) and eight source-structures (lentiform nucleus, cerebral cortex, thalamus, cerebral white matter, caudate nucleus, cerebellum, cerebral fluid and lateral ventricles). Ratios in a range of 0.21–10.39 were found for ICRP-HEAD phantom/MIRD-15 phantom, while ratios of 0.48–1.48 were found for ICRP-HEAD phantom/VIP-Man phantom. The highest difference (ratio of 10.39) was found in the caudate nucleus, with the lateral ventricles as the source-tissue. Most of S-values obtained from the MIRD-15 phantom for the thyroid, showed to be considerably higher than those obtained from the ICRP-HEAD phantom. A better agreement of S-values was found for the two voxelized phantoms (ICRP-HEAD and VIP-Man phantoms).

## 4. Discussion

A computational whole-body phantom for MCNP Monte Carlo code that includes a complete set of head and brain structures of relevance for neuroimaging studies, the ICRP-HEAD phantom, has been constructed from ICRP-110 adult male reference phantom and the Zubal head phantom. The ICRP-HEAD phantom is a multi-resolution phantom

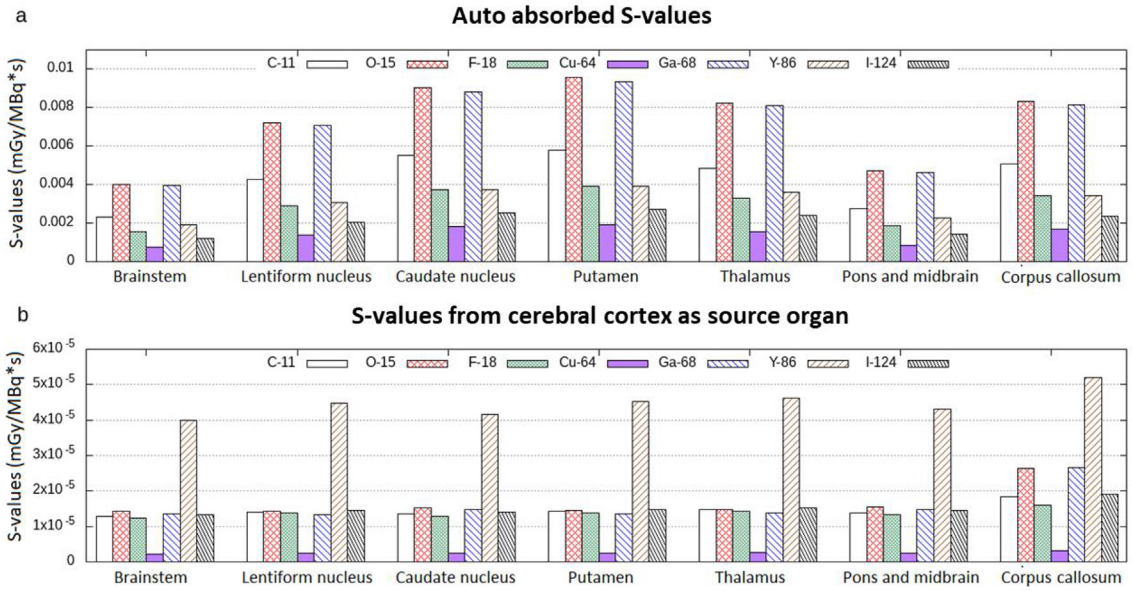


**Fig. 3.** (a) Auto absorbed S-values, and (b) S-values from cerebral cortex as source-organ for the seven positrons-emitted radionuclides.

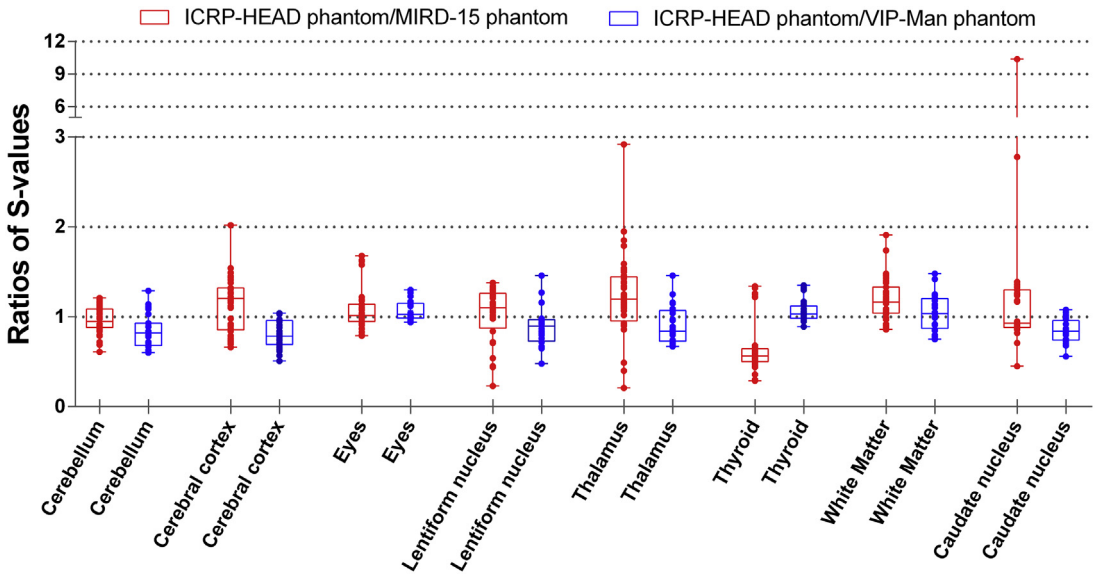


**Fig. 4.** Ratios of S-values of ICRP-HEAD phantom to stylized MIRD-15 phantom (red), and to VIP-Man phantom (blue). (For interpretation of the references to colour in this figure legend, the reader is referred to the Web version of this article.)

with a high resolution in the brain region that provides an accurate representation of cerebral structures, which could improve dose estimations by Monte Carlo simulations.

An advantage of the ICRP-HEAD phantom over other previously published head/brain phantoms, such as MIRD-15 phantom and VIP-Man head phantom, is that it includes a whole-body based on the ICRP-110 adult male reference phantom, which may be important not only for internal dosimetry but also for other medical physics applications. For this work, the body part of the phantom was used to calculate S-values in two important organs: the complete spinal cord (which extends from the medulla oblongata in the brainstem to the lumbar region of the vertebral column), and for the thyroid (which is an organ essential for dose estimations in nuclear medicine).

Although the ICRP-HEAD phantom has a high resolution in the head part and it is attached to the body part of the ICRP-110 phantom, the total number of voxels resulted well suited for Monte Carlo simulations in MCNP6.2 code with the parameters used and for the positron-emitting radionuclides studied in this work. Moreover, other parameters such as particle type, cut-off energy, tally type, beam energy, and the use of variance reduction techniques could modify its efficiency.

The SAFs for positrons and photons showed to be higher for structures with larger masses. However, the SAFs for electrons also showed a dependence on the shape of the structure as shown in Fig. 2. The SAFs for positrons, electrons, and photons decrease as the energy increases, because when the energy of the particles or photons increases, more of them escape from the source-structure. Two types of behavior were observed in the SAFs for the positrons: at low energies (less than 1 MeV), SAFs are higher than 1 because the positrons and some annihilation-gamma photons are absorbed in the source-structure; at higher energies (> 1 MeV), SAFs are less than 1 because some positrons come out of the source-structure, although some photons are absorbed in the source-structure, decreasing the absorbed energy.

S-values were calculated for seven positron emitting radionuclides, three commonly used in brain PET (F-18, C-11, and O-15) and four non-conventional radionuclides (Cu-64, I-124, Ga-68, and Y-86) with potential applications in neuroimaging (Diaz-Ruiz et al., 2017)(Cascini et al., 2014)(Banerjee and Pomper, 2013). O-15 and Ga-68 were the radionuclides with the highest auto absorbed S-values. This can be explained because, in addition to a high emission intensity, they have positrons with high energies (1.68 MeV, and 1.85 MeV respectively). Y-86 produced the highest S-values when the target-organs were different from the source-organs, because Y-86 has a high emission intensity of gamma photons that produce a high cross-irradiation. Cu-64 showed the lowest S-values for both auto absorbed and cross-irradiation, because its principal emission (57%) are Auger electrons of low energy (0.8 keV).

Significant differences were found when the S-values calculated from the ICRP-HEAD phantom were compared with those obtained from the stylized MIRD-15 phantom, while a better agreement was found with the S-values obtained from the VIP-Man phantom. Differences found with respect to MIRD-15 phantom are due to the fact that its structure was created by mathematical functions that do not achieve to accurately reproduce the shape of many brain structures, and therefore produce wrong S-values. On the other hand, the ICRP-HEAD phantom and the VIP-Man phantom resemble the shapes of brain structures in a more accurately and detailed manner because they were created with a voxelized structure from tomographic information. The use of the stylized MIRD-15 phantom produces a dose underestimation for structures such as cerebral white matter, thalamus, and cerebral cortex while for the thyroid, it produces an important dose overestimation.

## 5. Conclusion

The voxel resolution of the constructed ICRP-HEAD phantom was well suited for Monte Carlo simulations in MCNP6 code. This phantom provides an accurate representation of the head and brain structures, and it could be used to estimate the absorbed dose for several medical physics applications. The S-values obtained in this work could help to improve the accuracy of absorbed dose in brain and head structures for positron-emitting radionuclides used in PET neuroimaging.

## Acknowledgments

Carlos Alberto Reynoso-Mejía is a 'Doctorado en Ciencias Fisicomatemáticas' student at the Instituto Politécnico Nacional in Mexico.

## Appendix A. Supplementary data

Supplementary data to this article can be found online at https://doi.org/10.1016/j.radphyschem.2019.108427.

## References


Banerjee, S.R., Pomper, M.G., 2013. Clinical applications of gallium-68. Appl. Radiat. Isot. 76, 2–13. https://doi.org/10.1016/j.apradiso.2013.01.039.

Belinato, W., Santos, W.S., Perini, A.P., Neves, L.P., Caldas, L.V.E., Souza, D.N., 2017. Estimate of S-values for children due to six positron emitting radionuclides used in PET examinations. Radiat. Phys. Chem. 140, 51–56. https://doi.org/10.1016/j.radphyschem.2017.02.038.

Bolch, W.E., Eckerman, K.F., Sgouros, G., Thomas, S.R., 2009. MIRD pamphlet No. 21: a generalized schema for radiopharmaceutical dosimetry–standardization of nomenclature. J. Nucl. Med. 50, 477–484. https://doi.org/10.2967/jnumed.108.056036.

Bouchet, L.G., Bolch, W.E., Weber, D.A., Atkins, H.L., Poston, J.W., 1999. MIRD Pamphlet No. 15: radionuclide S values in a revised dosimetric model of the adult head and brain. Medical Internal Radiation Dose. J. Nucl. Med. 40, 62S–101S.

Caracappa, P.F., Rhodes, A., Fiedler, D., 2014. Multi-resolution voxel phantom modeling: a high-resolution eye model for computational dosimetry. Phys. Med. Biol. 59, 5261–5275. https://doi.org/10.1088/0031-9155/59/18/5261.

Cascini, G.L., Niccoli Asabella, A., Notaristefano, A., Restuccia, A., Ferrari, C., Rubini, D., Altini, C., Rubini, G., 2014. 2014. 124 iodine: a longer-life positron emitter isotope—new opportunities in molecular imaging. BioMed Res. Int. 1–7. https://doi.org/10.1155/2014/672094.

Chao, T.C., Xu, X.G., 2004. S-values calculated from a tomographic head/brain model for brain imaging. Phys. Med. Biol. 49, 4971–4984. https://doi.org/10.1088/0031-9155/49/21/009.

Diaz-Ruiz, A., Martinez-Rodriguez, E., Martinez, R., Avila-Rodriguez, M.A., Garcia, O., Rios, C., 2017. Basal ganglia uptake of 64Cu in Parkinson's disease patients compared to healthy subjects. J. Neurol. Sci. 381, 223–224. https://doi.org/10.1016/j.jns.2017.08.639.

Emami, B., Lyman, J., Brown, A., Cola, L., Goitein, M., Munzenrider, J.E., Shank, B., Solin, L.J., Wesson, M., 1991. Tolerance of normal tissue to therapeutic irradiation. Int. J. Radiat. Oncol. 21, 109–122. https://doi.org/10.1016/0360-3016(91)90171-Y.

Evans, J.F., Blue, T.E., Gupta, N., 2001. Absorbed dose estimates to structures of the brain and head using a high-resolution voxel-based head phantom. Med. Phys. 28, 780–786. https://doi.org/10.1118/1.1354997.

Jia, X., Yan, H., Gu, X., Jiang, S.B., 2012. Fast Monte Carlo simulation for patient-specific CT/CBCT imaging dose calculation. Phys. Med. Biol. 57, 577–590. https://doi.org/10.1088/0031-9155/57/3/577.

Kinase, S., Saito, K., 2007. Evaluation of self-dose S values for positron emitters in voxel phantoms. Radiat. Prot. Dosim. 127, 197–200. https://doi.org/10.1093/rpd/ncm344.

Loevinger, R., Budinger, T.F., Watson, E.E., 1991. MIRD primer for absorbed dose calculations. Soc. Nucl. Med.

Menzel, H.-G., Clement, C., DeLuca, P., 2009. ICRP Publication 110. Realistic reference phantoms: an ICRP/ICRU joint effort. A report of adult reference computational phantoms. Ann. ICRP 39, 1–164. https://doi.org/10.1016/j.icrp.2009.09.001.

My, D.T.K., Phuong, D.N., Loan, T.T.H., Van Nhon, M., 2010. Calculating the Dosimetry Distribution of Leksell Gamma Knife in Phantom Zubal Head by Using MCNP5. pp. 106–109. https://doi.org/10.1007/978-3-642-12020-6_26.

Segars, W.P., Sturgeon, G., Mendonca, S., Grimes, J., Tsui, B.M.W., 2010. 4D XCAT phantom for multimodality imaging research. Med. Phys. 37, 4902–4915. https://doi.org/10.1118/1.3480985.

Stabin, M.G., da Luz, L.C.Q.P., 2002. Decay data for internal and external dose assessment. Health Phys. 83, 471–475.

Stabin, M.G., Siegel, J.A., 2018. RADAR dose estimate report: a compendium of radiopharmaceutical dose estimates based on OLINDA/EXM version 2.0. J. Nucl. Med. 59, 154–160. https://doi.org/10.2967/jnumed.117.196261.

Tai, Y.F., 2004. Applications of positron emission tomography (PET) in neurology. J. Neurol. Neurosurg. Psychiatry 75, 669–676. https://doi.org/10.1136/jnnp.2003.028175.

Valentin, J., 2002. Basic anatomical and physiological data for use in radiological protection: reference values. ICRP Publ. 89 Ann. ICRP 32, 1–277. https://doi.org/10.1016/S0146-6453(03)00002-2.

Werner, C.J., Bull, J.S., Solomon, C.J., Brown, F.B., McKinney, G.W., Rising, M.E., Dixon, D.A., Martz, R.L., Hughes, H.G., Cox, L.J., Zukaitis, A.J., Armstrong, J.C., Forster, R.A., Casswell, L., 2018. MCNP Version 6.2 Release Notes. Los Alamos, NM (United States). https://doi.org/10.2172/1419730.

White, D.R., Griffith, R.V., Wilson, I.J., 1992. Report 46. J. Int. Comm. Radiat. Units Meas. os24 NP-NP. https://doi.org/10.1093/jicru/os24.1.Report46.

Xie, T., Zaidi, H., 2016. Development of computational pregnant female and fetus models and assessment of radiation dose from positron-emitting tracers. Eur. J. Nucl. Med. Mol. Imaging 43, 2290–2300. https://doi.org/10.1007/s00259-016-3448-8.

Xu, X., Eckerman, K., 2009. Handbook of anatomical models for radiation dosimetry, series in medical physics and biomedical engineering. Taylor & Francis. https://doi.org/10.1201/EBK1420059793.

Zubal, I.G., Harrell, C.R., Smith, E.O., Rattner, Z., Gindi, G., Hoffer, P.B., 1994. Computerized three-dimensional segmented human anatomy. Med. Phys. 21, 299–302. https://doi.org/10.1118/1.597290.